ISSN 1392-3730/eISSN 1822-3605

VILNIUS TECH
Vilnius Gediminas Technical University

JOURNAL of CIVIL ENGINEERING and MANAGEMENT

2024
Volume 30
Issue 6
Pages 520–535
https://doi.org/10.3846/jcem.2024.21636

AN IMPROVED RANDOM FOREST MODEL TO PREDICT BOND STRENGTH OF FRP-TO-CONCRETE

Li TAO[1], Xinhua XUE[2]✉

[1]*School of Civil Engineering & Architecture, Wenzhou Polytechnic, Wenzhou 325000, P.R. China*
[2]*College of Water Resource and Hydropower, Sichuan University, Chengdu 610065, P.R. China*

Article History:
- received 19 November 2023
- accepted 17 March 2024

Abstract. Fiber-reinforced polymer (FRP) is an excellent building material for strengthening concrete structures, but it is difficult to accurately evaluate the bond strength of FRP-to-concrete due to the influence of various parameters. In this study, a novel hybrid model which combines particle swarm optimization (PSO) with random forest (RF) was proposed to predict the bond strength of FRP-to-concrete. The PSO algorithm was used to optimize the hyperparameters of the RF model. A total of 749 specimens collected from the literature were used to develop the proposed PSO-RF model. Each sample contains 11 parameters required for the model. These 11 parameters are (1) the compressive strength of concrete, (2) the tensile strength of concrete, (3) the width of concrete specimen, (4) the maximum aggregate size of concrete, (5) the tensile strength of FRP, (6) the thickness of FRP, (7) the elastic modulus of FRP, (8) the tensile strength of adhesive, (9) the bond length of FRP, (10) the bond width of FRP, and (11) the bond strength of FRP-to-concrete. The proposed PSO-RF model was compared with other machine learning models as well as ten empirical equations. Six statistical indices, namely root mean squared error (RMSE), mean absolute error (MAE), coefficient of determination (R^2), Nash-Sutcliffe efficiency coefficient (NSE), Willmott's Index of Agreement (WIA), and Legates-McCabe's Index (LM) were used to evaluate the prediction performance of the abovementioned models. The results show that the RMSE, MAE, R^2, NSE, WIA and LM values of the PSO-RF model are 1.529 kN, 0.942 kN, 0.986, 0.984, 0.996 and 0.892, respectively, for the training datasets and 2.672 kN, 1.967 kN, 0.963, 0.961, 0.989 and 0.761, respectively, for the test datasets. It can be concluded that the proposed PSO-RF model has the best comprehensive performance in predicting the bond strength of FRP-to-concrete. In addition, the sensitivity analysis of the PSO-RF model was also conducted in this study.

Keywords: fiber-reinforced polymer, multivariate adaptive regression splines, wavelet neural network, particle swarm optimization, random forest.

✉Corresponding author. E-mail: *scuxxh@163.com*

1. Introduction

Fiber-reinforced polymer (FRP) composites have the advantages of fatigue resistance, high tensile strength, good corrosion resistance and low thermal conductivity, and are excellent building materials for strengthening concrete structures. In recent years, FRP composites have been widely used in buildings, tunnel linings, bridges and marine structures (Chróścielewski et al., 2019; Siwowski et al., 2019).

In the FRP-concrete bonding systems, the bond strength of FRP-concrete is affected by many parameters, including the properties of FRP materials, binders and concrete (e.g., compressive strength and maximum aggregate size of concrete; thickness of FRP, bond length and width, tensile strength of adhesive, etc.) (Zhang & Wang, 2021). In recent years, scholars have done a lot of research on the bond mechanism of FRP reinforced concrete. For example, Irshidat and Al-Saleh (2016) studied the bond slip performance between FRP sheets and concrete surfaces. Ozakkaloglu et al. (2017) studied the influence of FRP on the performance of concrete members. Czaderski et al. (2010) conducted a pull-out bond test between FRP and concrete. Pan and Leung (2017) studied the bond ability of FRP/ concrete through direct shear tests. Although many experiments can be carried out in the laboratory to evaluate the bond strength of FRP-to-concrete, it is impossible to accurately evaluate the bond strength of FRP-to-concrete due to the influence of various parameters.

With recent developments in computational software and hardware, many artificial intelligence (AI) techniques have grown at a remarkable rate, attracting a great number of researches and practitioners. To date, artificial neural networks (ANNs), fuzzy logic, adaptive neuro-fuzzy

inference system (ANFIS), support vector machine (SVM), least squares support vector machine (LSSVM), M5 model tree (M5MT), multivariate adaptive regression splines (MARS), random forest (RF), random tree (RT), etc., and their combinations with evolutionary algorithms are the main strategies of soft computing. An evolutionary algorithm is a type of artificial intelligence that is driven by optimization processes we observe in nature, such as natural selection, species migration, bird swarms, human culture, and ant colonies. Featured evolutionary algorithms include genetic algorithms (GAs), genetic programming (GP), evolution strategies, evolutionary programming, ant colony optimization, particle swarm optimization (PSO), differential evolution, simulated annealing, biogeography-based optimization, and so on.

Due to their strong ability to capture nonlinear relationships among high-dimensional variables, AI techniques have been widely used to predict the bond strength of FRP-to-concrete (Cascardi et al., 2017; Zhang & Wang, 2021; Jahangir & Eidgahee, 2021; Chen et al., 2021; Pei & Wei, 2022; Zhang et al., 2023). For example, Zhang and Wang (2021) developed a metaheuristic-optimized least squares support vector regression model to predict the bond strength between FRP and concrete. Cascardi et al. (2017) proposed an ANN-based analytical model to estimate the compressive strength of concrete columns constrained by FRP. Jahangir and Eidgahee (2021) developed a hybrid artificial bee colony algorithm-ANN model to predict the FRP-concrete bond strength. Zhang et al. (2023) predicted the FRP-concrete interfacial bond strength using six machine learning models. Pei and Wei (2022) investigated the bond strength of FRP-to-concrete under direct tension by ant colony optimization-based ANFIS approach.

In view of the above, as well as the author's understanding, little research so far has dealt with the hybrid model which combines particle swarm optimization (PSO) and random forest (RF) for predicting the bond strength of concrete under FRP confinement. Therefore, this study presents a novel hybrid PSO-RF model to predict the bond strength of FRP-to-concrete. The PSO algorithm was used to optimize the hyperparameters of the RF model. To evaluate the performance of the proposed PSO-RF model, it was compared with other machine learning models as well as 10 empirical equations.

The rest of the article is arranged as follows: Section 2 introduces the data sets used to develop the models. Section 3 describes the principles of the proposed PSO-RF model, as well as other machine learning models and the existing empirical equations. Section 4 presents the results and discussion. The final conclusions are presented in Section 5.

2. Data collection

In this study, experimental data of 749 specimens were collected from literature (Bakis et al., 1998; Dai et al., 2005; Daud et al., 2015, 2017; Garzon-Roca et al., 2015; Haddad et al., 2015; Hadigheh et al., 2015; Peng et al., 2015; Ghorbani et al., 2017; Al-Saadi et al., 2018; Barris et al., 2018; Nerilli & Vairo, 2018; Wan et al., 2018; Ascione et al., 2019; Barham et al., 2019; Correial et al., 2019; Murad et al., 2019; Yuan et al., 2019; Alam et al., 2020) to establish the model. Each sample contains 11 parameters required for the model. These 11 parameters are (1) the compressive strength of concrete f_c, (2) the tensile strength of concrete f_t, (3) the width of concrete specimen b_c, (4) the maximum aggregate size of concrete D_{max}, (5) the tensile strength of FRP f_{Ft}, (6) the thickness of FRP t_f, (7) the elastic modulus of FRP E_f, (8) the tensile strength of adhesive f_{At}, (9) the bond length of FRP L, (10) the bond width of FRP b_f, and (11) the bond strength of FRP-to-concrete P_u.

To develop statistical and machine learning models, datasets are typically divided into two parts: training and testing. The training part is used to fit the model, that is, to estimate the unknown parameters in the model. The accuracy of the model is then assessed using the test data set. The reason for this is that if we use the entire data set for fitting, then the model will overfit the data and may lead to poor predictions for future scenarios. Therefore, keeping a portion of the data set and testing its performance before deploying the model to the field can prevent unexpected problems due to overfitting. The training/testing division can be done randomly or in a fixed manner. The fixed approach is usually avoided because it may introduce systematic differences between the training set and the test set, leading to sample representativeness issues. To avoid such systematic differences, randomly assigning instances to the training data set is often used. In this study, 566 out of 749 datasets were randomly selected as the training datasets while the remaining 183 were used for testing.

The statistical results of 749 specimens are listed in Table 1. The Pearson correlation coefficients between different parameters are shown in Table 2. Figure 1 plots the

Table 1. Statistical results of the experimental data

Parameter	f_c (MPa)	f_t (MPa)	b_c (mm)	D_{max} (mm)	f_{Ft} (MPa)	t_f (mm)	b_f (mm)	E_f (GPa)	f_{At} (MPa)	L (mm)	P_u (kN)
Maximum	76	6.3	500	32	4900	8	200	425.1	65	1200	123.72
Minimum	13	1.02	50	4.75	196	0.039	10	22.5	10	20	1.62
Mean	34.32	3.34	155.92	15.54	3283.91	0.59	66.12	205.34	290.2	189.06	21.09
Median	34	3.34	150	15	3525	0.17	50	230	30	150	19.99
Standard deviation	10.46	0.79	47.52	4.13	983.95	0.81	34.35	60.39	9.69	126.39	12.53

histogram frequencies of eight parameters (e.g., f_c, f_t, D_{max}, f_{At}, E_f, t_f, L, b_f). It can be seen from Figure 1 that the distributions of the parameters are similar, and they can fully extend the development of the models. As can be seen from Table 2, the thickness, bond width, length, tensile strength and elastic modulus of FRP have great influence on the bond strength of FRP and concrete. Among them, the bond width of FRP has the most significant effect on bond strength.

3. Methodology

3.1. Particle swarm optimization (PSO)

The PSO algorithm is inspired by simulating the social behaviors of birds such as flight and foraging. It is a swarm intelligence algorithm, which obtains the optimal state through information interaction between the group and the individual. Each particle is a potential solution, and each group contains a group of particles. The principle of PSO algorithm is to initialize a set of random particles with random solutions, and then find the global optimal solution through repeated iterative computation. The main steps of PSO are as follows (Luat et al., 2021):

1) Particle swarm initialization. In d-dimensional space, the velocity interval and search space after particle swarm initialization are determined by chaotic mapping method. The initial position of each particle is then evenly distributed. The velocity determines the distance and path of each particle, which can be updated by Eqn (1):

$$\upsilon_{id}^{k+1} = w\upsilon_{id}^{k} + a_1 r_1\left(P_{id}^{k} - x_{id}^{k}\right) + a_2 r_2\left(G_d^{k} - x_{id}^{k}\right), \quad (1)$$

where w is the non-negative inertia weight; υ_{id}^{k}, P_{id}^{k} and x_{id}^{k} represent the velocity, individual extremum and the position of particle i in the d-dimensional search space after the kth iteration, respectively. a_1 and a_2 are non-negative acceleration coefficients, r_1 and r_2 are two random numbers between 0 to 1. G_d^k is the historical global best position in the d-dimensional search space after the kth iteration.

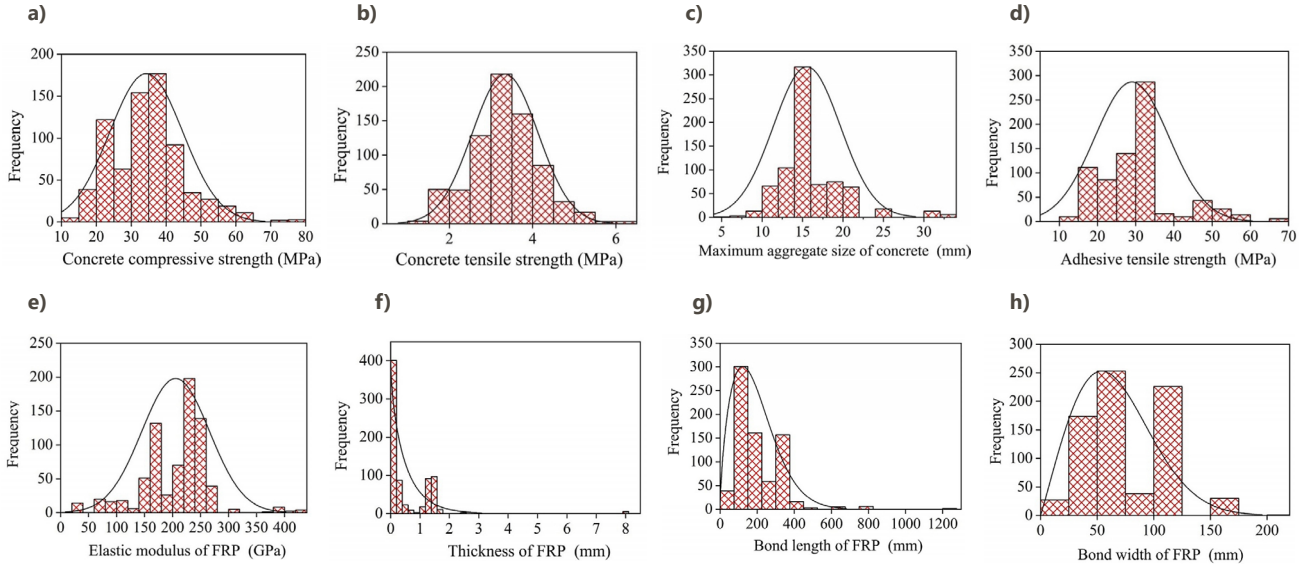

Figure 1. Histograms of the eight parameters

Table 2. Pearson correlation coefficients between different parameters

	P_u	f_c	f_t	b_c	D_{max}	f_{Ft}	t_f	E_f	f_{At}	L	b_f
P_u	1	--	--	--	--	--	--	--	--	--	--
f_c	.058	1	--	--	--	--	--	--	--	--	--
f_t	–.023	.532**	1	--	--	--	--	--	--	--	--
b_c	.148**	.001	–.077*	1	--	--	--	--	--	--	--
D_{max}	–.100**	–.068	.001	–.059	1	--	--	--	--	--	--
f_{Ft}	–.333**	–.116**	–.007	–.087*	.106**	1	--	--	--	--	--
b_f	.688**	.104**	.017	.089*	–.139**	–.522**	1	--	--	--	--
E_f	–.300**	–.007	.032	–.215**	.125**	.676**	–.502**	1	--	--	--
f_{At}	–.163**	.054	–.047	–.161**	.034	.166**	–.227**	.164**	1	--	--
L	.390**	.068	–.130**	.133**	–.008	–.254**	.278**	–.204**	–.068	1	--
t_f	.533**	–.123**	–.112**	.197**	.101**	.141**	–.086*	.022	.025	.031	1

Note: ** and * indicate significant correlation at the 0.01 and 0.05 levels (two-tailed), respectively.

2) Determine the extreme value of each particle, that is, the best position of particle *i*. The fitness value f_i of particle *i* is calculated and then compared with the extreme value P_i of that particle. If $f_i \geq P_i$, replace P_i with f_i.

At the beginning of iterative calculation of PSO, it is necessary to improve the global search ability of PSO. In iterative calculation, the inertia weight *w* is generally determined by a linear decline function. In order to avoid premature convergence of particle swarm under finite iteration conditions, dynamic adaptive inertial weights are used to find the global optimal position by balancing global and local search capabilities, as defined in Eqn (2).

$$w = \begin{cases} w_{\min} - \dfrac{(w_{\max} - w_{\min})(f - f_{\min})}{f_{avg} - f_{\min}} & f \leq f_{avg} \\ w_{\max} & f > f_{avg} \end{cases}, \quad (2)$$

where *f* is the current fitness value of the particle *i*, *w* is the inertia weight coefficient.

3) Determine the historical global optimal position of a particle swarm. Compare the global extreme value *G* with the fitness value *f* of particle *i*, replace *G* with f_i if $f_i \geq G$.

4) Update the position and velocity of each particle. The position update formula of random particles is shown in Eqn (3).

$$x_{id}^{k+1} = x_{id}^{k} + \upsilon_{id}^{k+1}. \quad (3)$$

5) Determine whether the PSO algorithm is terminated. If the global optimal position of particle swarm is found, the algorithm ends, otherwise return to step (2).

3.2. Random forest (RF)

RF, first proposed by Breiman (2001), refers to a classifier that uses multiple trees to train and predict samples. Due to its remarkable characteristics of good robustness and strong generalization ability, RF has been widely used in many fields (Nilsen et al., 2019; Naser et al., 2021). RF is a supervised learning method that builds decision trees on data samples, generates and accumulates predictions for each sample, and then votes on the best of them. When developing an RF model, there are two hyperparameters that need to be determined, namely the depth of the decision tree and the number of decision trees. The RF algorithm is briefly described as follows (Daneshvar & Behnood, 2020):

1) The bagging method is used to randomly extract samples from the original training set and construct *k* sample subsets.

2) Using the random subspace method, *F* features are randomly extracted from all *X* feature attributes for node splitting, and the regression decision tree is constructed.

3) Based on the concept of ensemble learning, the output of each regression decision tree is averaged to obtain the prediction results, as shown in Eqn (4):

$$\bar{h}_{\mathrm{RF}}(x) = \frac{1}{T}\sum_{t=1}^{T}\{h(\theta_t, x)\}, \quad (4)$$

where $\bar{h}_{\mathrm{RF}}(x)$ represents the predicted result, *T* represents the number of regression decision trees, $h(\theta_t, x)$ represents the output based on θ_t and *x*, θ_t represents an independent and identically distributed random vector, and *x* represents an independent variable.

The flowchart of the RF model is shown in Figure 2.

3.3. PSO-RF

Traditional RF algorithms require a lot of trial and error to determine the hyperparameters. PSO algorithm has the advantages of strong generality, independent information and easy implementation. Therefore, PSO algorithm was used to determine the hyperparameters n_{tree} and p_{try} of the RF model in this study.

The PSO-RF model framework consists three stages: data processing, RF model training and testing. In the data processing stage, 566 datasets were randomly selected from 749 datasets as training datasets, and the remaining 183 datasets were used for testing. In the training stage, the optimal RF model is determined by searching the optimal hyperparameters n_{tree} and p_{try} using the PSO algorithm. Firstly, the initial position and velocity of the particles are randomly assigned, and the corresponding RF model hyperparameters are specified. After calculating the fitness of each round, the local optimal position and the global optimal position of the particle swarm are determined. Since the position and velocity of the particle are dynamic, the best RF model can be obtained when the number of iterations reaches the maximum and the fitness value is unchanged. In the testing stage, the optimal RF model was evaluated by the test datasets. The steps for PSO to optimize RF model are as follows (Dai et al., 2022):

1) According to the characteristics of the samples, the particle swarm parameters are initialized and the position and velocity vectors of the particle swarm are determined.

2) Evaluate the fitness values for all particles. In this study, the root mean squared error (RMSE) was determined as the fitness function.

3) Update the velocity and position of each particle.

4) When the number of iterations is maximum and the fitness is constant, the optimal hyperparameters of the RF model can be obtained.

The flowchart of the hybrid PSO-RF model is shown in Figure 3.

3.4. Group method of data handling (GMDH)

Since GMDH was proposed by Ivakhnenko (1971), it has been widely used in different fields. A typical GMDH conceptual structure consists of one output neuron (Y_1) and four input parameters (X_1~X_4), as shown in Figure 4. The layers in the network can be divided into the following three parts: the input layer, the hidden layer, and the output layer.

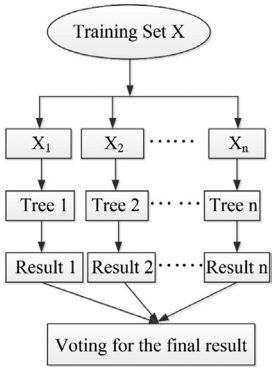

Figure 2. Flowchart of RF algorithm

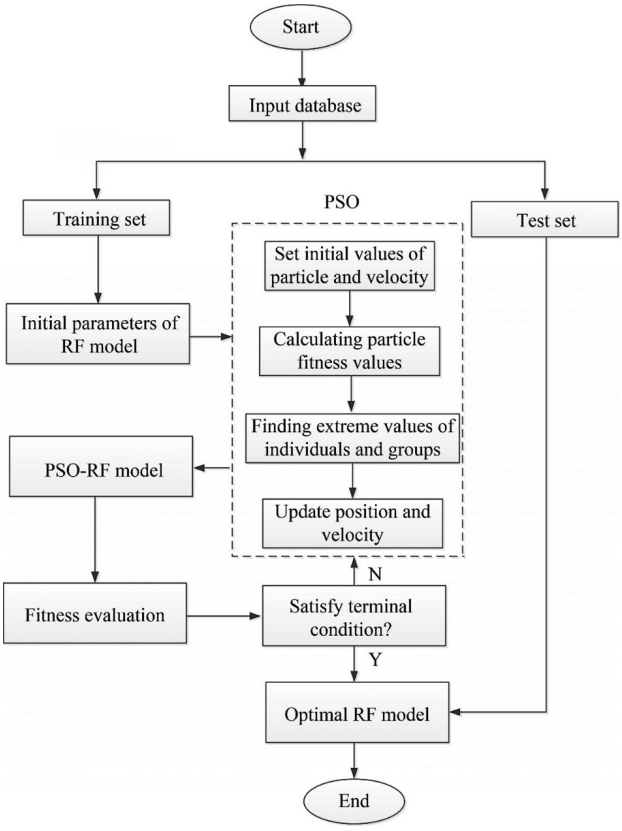

Figure 3. Flowchart of the hybrid PSO-RF algorithm

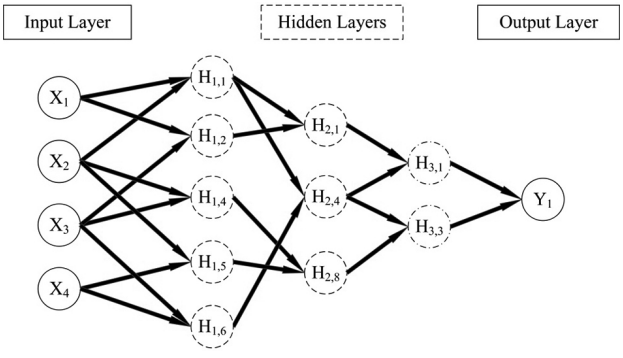

Figure 4. Structure of GMDH model

First, neurons in the first hidden layer are created by combining each neuron with other neurons in the input layer. The generation of new neurons in the next layer requires that the relationship between each pair of neurons in the previous layer satisfy the Ivakhnenko polynomial (Ivakhnenko, 1971):

$$H_{k,m} = C_1 + C_2 H_{k-1,i} + C_3 H_{k-1,j} + C_4 H_{k-1,i}^2 + C_5 H_{k-1,j}^2 + C_6 H_{k-1,i} H_{k-1,j}, \quad (5)$$

where $H_{k,m}$ represents the value of the mth neuron in the kth layer; $H_{k-1,i}$ and $H_{k-1,j}$ represent the output values of the ith and jth neurons in the (k-1)th layer, respectively; C_1~C_6 are polynomial coefficients.

Replace $H_{k,m}$ with the target value y; thus, Eqn (5) can be recalculated as Eqn (6):

$$\begin{pmatrix} 1 & H_{k-1,i,1} & H_{k-1,j,1} & H_{k-1,i,1}^2 & H_{k-1,j,1}^2 & H_{k-1,i,1} H_{k-1,j,1} \\ \vdots & \vdots & \vdots & \vdots & \vdots & \vdots \\ 1 & H_{k-1,i,n} & H_{k-1,j,n} & H_{k-1,i,n}^2 & H_{k-1,j,n}^2 & H_{k-1,i,n} H_{k-1,j,n} \end{pmatrix} \begin{pmatrix} C_1 \\ C_2 \\ C_3 \\ C_4 \\ C_5 \\ C_6 \end{pmatrix} = \begin{pmatrix} Y_1 \\ \vdots \\ Y_n \end{pmatrix}. \quad (6)$$

The selection of neurons is based on the RMSE corresponding to the output value of each pair of neurons. The RMSE of all coupled neurons in the same layer is calculated and compared with the preset threshold, and then the coupled neurons whose RMSE value is higher than the preset threshold are eliminated. If the calculated RMSE value meets the requirements, it is retained. Therefore, it is necessary to set the threshold of RMSE in advance to select a pair of neurons. The calculation process of RMSE error threshold can be described by Eqns (7) and (8). Finally, the neuron with the smallest RMSE value is selected as the output value of GMDH model. Figure 5 shows the selection process of neurons.

$$\mathrm{RMSE}_{H_{k,m}} = \sqrt{\frac{1}{n}\sum_{v=1}^{n}\left(H^v{}_{k,m} - y^v\right)^2}; \quad (7)$$

$$T = 0.6\mathrm{Min}\left(\mathrm{RMSE}_{H_{k,m}}\right) + 0.4\mathrm{Max}\left(\mathrm{RMSE}_{H_{k,m}}\right), \quad (8)$$

where $H_{k,m}$ and y represent the measured and predicted values, respectively, n represents the number of samples, T represents the preset threshold.

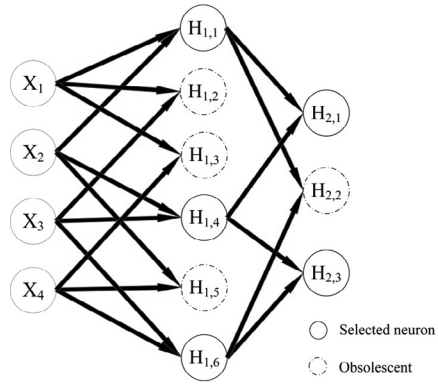

Figure 5. The selection of neurons in GMDH model

Therefore, the general relationship between the output variables and the input parameters can be expressed by the Ivankhnenko polynomial, as shown in Eqn (9):

$$Y_1 = f\left(X_1, X_2, X_3, \ldots\right) = C_0 + \sum_{i=1}^{n} C_i X_i + \sum_{j=1}^{n}\sum_{i=1}^{n} C_{ij} X_i X_j + \sum_{k=1}^{n}\sum_{j=1}^{n}\sum_{i=1}^{n} C_{ijk} X_i X_j X_k + \ldots, \quad (9)$$

where $X_1, X_2, X_3, \ldots$ are the input parameters; $C_0, C_i, C_{ij}, C_{ijk}, \ldots$ are the polynomial coefficients; i, j, k represent the indices of the input components, n is the number of input points, and Y_1 represents the estimated output variable.

3.5. Multivariate adaptive regression splines (MARS)

MARS was first proposed by Friedman (1991). As a nonlinear non-parametric regression method, MARS models the nonlinear relationship between different variables through a series of piecewise linear splines of different gradients. Considering the general model form of the relationship between the input x and the target output y as follows (Friedman, 1991):

$$y = f\left(x\right) = a_0 + \sum_{m=1}^{M} a_m B_m\left(x\right), \quad (10)$$

where a_0 is a constant; a_m is the coefficient of basis functions (BFs) B_m.

According to Friedman (1991), MARS uses the following bilateral truncated power functions as the spline BFs:

$$b_q^{\pm}\left(x-t\right) = \left[\pm\left(x-t\right)\right]_+^q, \quad (11)$$

where t is the knot location, q is the order of the spline.

The analysis of variance decomposition of the MARS model is given by the following equation (Friedman, 1991):

$$f\left(x\right) = a_0 + \sum_{K_m=1} f_i\left(x_i\right) + \sum_{K_m=2} f_{ij}\left(x_i, x_j\right) + \sum_{K_m=3} f_{ijk}\left(x_i, x_j, x_k\right) + \ldots. \quad (12)$$

The first sum $\sum_{K_m=1} f_i\left(x_i\right)$ is over all BFs that involve only a single variable. The second sum $\sum_{K_m=2} f_{ij}\left(x_i, x_j\right)$ is over all BFs that involve exactly two variables. Similarly, the third sum $\sum_{K_m=3} f_{ijk}\left(x_i, x_j, x_k\right)$ represents (if present) the contributions from three variable interactions.

Equation (12) involves the sum of the product of functions, and the form is similar to the following (Friedman, 1991):

$$b\left(x|s,t\right) = \left[s\left(x-t\right)\right]_+. \quad (13)$$

To solve this problem, the strategy is to replace each such function with a corresponding truncated cubic function of the form (Friedman, 1991):

$$BF\left(x \mid s=+1, t_-, t, t_+\right) = \begin{cases} 0 & x \le t_-, \\ p_+\left(x-t_-\right)^2 + r_+\left(x-t_-\right)^3 & t_- < x < t_+, \\ x-t & x \ge t_+, \end{cases}$$

$$BF\left(x \mid s=-1, t_-, t, t_+\right) = \begin{cases} -\left(x-t\right) & x \le t_-, \\ p_-\left(x-t_+\right)^2 + r_-\left(x-t_+\right)^3 & t_- < x < t_+, \\ 0 & x \ge t_+ \end{cases} \quad (14)$$

with $t_- < x < t_+$. Setting

$$\begin{aligned} p_+ &= \left(2t_+ + t_- - 3t\right) \Big/ \left(t_+ - t_-\right)^2, \\ r_+ &= \left(2t - t_+ - t_-\right) \Big/ \left(t_+ - t_-\right)^3, \\ p_- &= \left(3t - 2t_- - t_+\right) \Big/ \left(t_- - t_+\right)^2, \\ r_- &= \left(t_- + t_+ - 2t\right) \Big/ \left(t_- - t_+\right)^3 \end{aligned} \quad (15)$$

causes $BF\left(x \mid s, t_-, t, t_+\right)$ to be continuous and have continuous first derivatives. More details of MARS can be found in Friedman (1991).

3.6. Wavelet neural network (WNN)

WNN was first proposed by Zhang and Benveniste (1992). WNN combines the advantages of wavelet transform and neural network, and uses wavelet function instead of sigmoid activation function as activation function. Compared with other neural networks, WNN has the following advantages: (i) it is easier to obtain hidden nodes and weights than radial basis function neural networks; (ii) fewer iterations than multilayer perceptron network, and (iii) faster convergence. Due to its good capability of learning and excellent performance, WNN model was adopted in this study. The architecture of WNN is shown in Figure 6.

In Figure 6, x_1, x_2, ... , x_m are the input variables, y_1, y_2, ... , y_s are the output variables, w_{ij} and w_{jk} are the weights connecting every layer. The shift factor and stretch factor of hidden layer are a_j and b_j, respectively. The Morlet wavelet (ψ_j) is used as the mother wavelet function. The jth input of wavelet neuron in the hidden layer is calculated as (Zhang & Benveniste, 1992):

$$h_j = \sum_{i=1}^{m} x_i w_{ij} \quad j = 1, 2, \ldots, n. \quad (16)$$

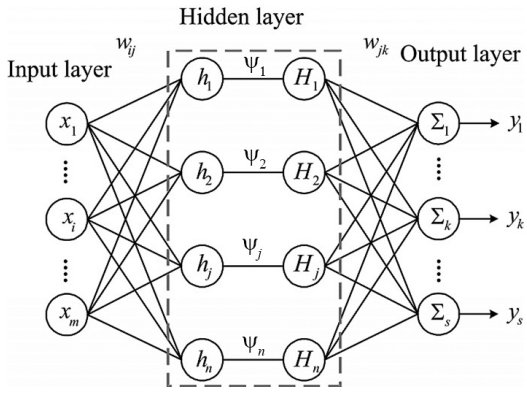

Figure 6. The architecture of WNN

After the wavelet transform, the *j*th output of wavelet neuron in the hidden layer can be calculated as (Zhang & Benveniste, 1992):

$$H_j = \psi_j\left(h_j\right) = \exp\left[-0.5\left(\frac{h_j - b_j}{a_j}\right)^2\right] \cdot \cos\left[1.75\left(\frac{h_j - b_j}{a_j}\right)\right]. \quad (17)$$

Then, the predicted value of the *k*th node in the output layer is written as (Zhang & Benveniste, 1992):

$$y_k = \sum_{j=1}^{n} H_j w_{jk}, \quad k = 1, 2, ..., s. \quad (18)$$

More details of WNN can be found in Zhang and Benveniste (1992).

3.7. Gene expression programming (GEP)

As an updated form of genetic algorithm, the individuals in the GEP model are designed to be linear strings of a certain length (genomes or chromosomes). The advantage of GEP is its powerful search and evolution capabilities. It can discover mathematical expressions that are most suitable for modeling data, based entirely on experimental data, without prior knowledge of the underlying laws. According to Ferreira (2001), a chromosome contains one or more gens, and each gene is composed of a head and a tail. Both the functions and terminals are stored in the head of the gene, while the tail contains only the terminals. Therefore, there are two languages in GEP, that is, the language of expression trees and the language of genes. Figure 7 shows a simple example of the conversion between these two languages.

The main steps of GEP establishment are summarized as follows:

1) Select the appropriate fitness function. In this study, the following formula is adopted as the fitness value:

$$f_i = 1000\left[1 + \sqrt{\frac{1}{m}\sum_{j=1}^{m}\left(Y_{i,j} - X_i\right)^2}\right]^{-1}, \quad (19)$$

where f_i is the fitness value and it ranges from 0 to 1000 (ideally, the fitness value is 1000); m is the total number of chromosomes; $Y_{i,j}$ and x_i represent the value predicted by the individual chromosome i for fitness case j and the monitored value for fitness case i, respectively.

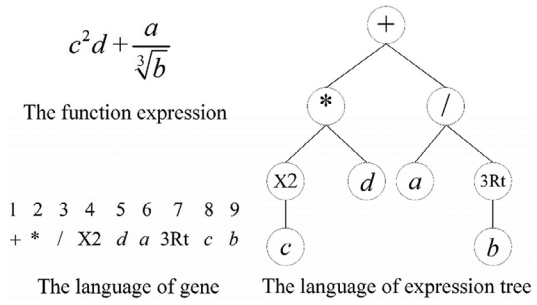

Figure 7. Schematic diagrams of the two languages

2) Select the type of linking function. In this study, the linking function of multiplication was selected because it can provide better results than other linking functions.

3) Select the genetic operators. In this study, the selection of genetic operators is mainly based on the research results of Ferreira (2001), and the selected genetic operators are listed in Table 4.

More details of GEP can be found in Ferreira (2001).

3.8. Existing empirical models

In this study, ten empirical models available in the literature were used to estimate the bond strength of concrete under FRP confinement, which were then compared with the results of the abovementioned machine learning models. Table 3 summarizes ten empirical models collected in this study for comparison.

3.9. Performance evaluation

In this study, six statistical indices, root mean squared error (RMSE), mean absolute error (MAE), coefficient of determination (R^2), Nash-Sutcliffe efficiency coefficient (NSE) (Nash & Sutcliffe, 1970), Willmott's Index of Agreement (WIA) (Willmott et al., 1981), and Legates-McCabe's Index (LM) (Legates & McCabe, 1999) were used to evaluate the prediction performance of the abovementioned models:

$$\text{RMSE} = \sqrt{\frac{1}{n}\left(\sum_{i=1}^{n}\left(y_{pred,i} - y_{obs,i}\right)^2\right)}; \quad (20)$$

$$\text{MAE} = \frac{1}{n}\sum_{i=1}^{n}\left|y_{pred,i} - y_{obs,i}\right|; \quad (21)$$

$$\text{R}^2 = 1 - \frac{\sum_{i=1}^{n}\left(y_{obs,i} - y_{pred,i}\right)^2}{\sum_{i=1}^{n}\left(y_{obs,i} - \bar{y}_{obs}\right)^2}; \quad (22)$$

$$\text{NSE} = 1 - \frac{\sum_{i=1}^{n}\left(y_{pred,i} - y_{obs,i}\right)^2}{\sum_{i=1}^{n}\left(y_{obs,i} - \bar{y}_{obs}\right)^2}; \quad (23)$$

$$\text{WIA} = 1 - \frac{\sum_{i=1}^{n}\left(y_{pred,i} - y_{obs,i}\right)^2}{\sum_{i=1}^{n}\left(\left|y_{pred,i} - \bar{y}_{obs}\right| + \left|y_{obs,i} - \bar{y}_{obs}\right|\right)^2}; \quad (24)$$

$$\text{LM} = 1 - \left[\frac{\sum_{i=1}^{n}\left|y_{pred,i} - y_{obs,i}\right|}{\sum_{i=1}^{n}\left|y_{obs,i} - \bar{y}_{obs}\right|}\right], \quad (25)$$

where $y_{pred,i}$ and $y_{obs,i}$ represent the predicted and observed results, respectively. $\bar{y}_{obs}$ is the average value of the observed results, n represents the total sample size.

Table 3. Summary of ten existing models

Model	Formula
Hiroyuki and Wu (1997)	$P_u = 5.88L^{-0.669}b_f L$
Maeda et al. (1999)	$L_e = \min\begin{Bmatrix} L \\ \exp\left[6.13 - 0.580\ln\left(E_f t_f \times 10^{-3}\right)\right] \end{Bmatrix}; P_u = 110.2\times10^{-6}E_f t_f b_f L_e$
Japan Concrete Institute [JCI] (2003)	$L_e = \min\begin{Bmatrix} L \\ 0.128\left(E_f t_f\right)^{0.57} \end{Bmatrix}; P_u = 0.93 f_c^{0.44} b_f L_e$
Dai et al. (2005)	$G_c = 0.514 f_c^{0.236}; P_u = \left(b_f + 7.4\right)\sqrt{2G_c E_f t_f}$
Accardi et al. (2007)	$P_u = b_f f_c^{0.25}\sqrt{12E_f t_f}$
Khalifa et al. (1998)	$P_u = 110.2\times10^{-6}\times\left(\frac{0.79f_c}{42}\right)^{2/3}\times E_f \times t_f \times b_f \times l_e$
Niedermeier (1996)	$G_c = 0.514 f_c^{0.236};\ L_e = \sqrt{\frac{E_f t_f}{0.5 f_t}};\ \alpha = \begin{cases} \left(\frac{L}{L_e}\right)\cdot\left(2 - \frac{L}{L_e}\right), L < L_e \\ , L \geq L_e \end{cases};\ P_u = 0.78\alpha b_f\sqrt{2G_c E_f t_f}$
Yang et al. (2001)	$L_e = \min\begin{Bmatrix} L \\ 100(\text{mm}) \end{Bmatrix};\ P_u = 0.5 f_t b_f L_e\left(0.5 + 0.08\sqrt{\frac{E_f t_f}{100 f_t}}\right)$
Neubauer and Rostásy (1997)	$k_p = \sqrt{1.125\frac{2 - b_f/b_c}{1 + b_f/400}};\ P_u = 0.64 k_p \alpha b_f\sqrt{f_t E_f t_f}$
Chen and Teng (2001)	$\beta_P = \sqrt{\frac{2 - b_f/b_c}{1 + b_f/b_c}};\ L_e = \sqrt{\frac{E_f t_f}{\sqrt{f_c}}};\ \beta_L = \begin{cases} \sin\frac{\pi L}{2L_e}, L < L_e \\ , L \geq L_e \end{cases};\ P_u = 0.427\beta_p\beta_L b_f L_e\sqrt{f_c}$

It should be noted that both RMSE and MAE have the same scales as the dataset. However, RMSE is more concerned with outliers. The NSE is ranging from $-\infty$ to 1. The closer the NSE is to 1, the better the performance of the model. Specifically, an NSE value between 0.75 and 1.0 is considered "very good", 0.65 to 0.75 is "good", 0.50 to 0.65 is "satisfactory", 0.4 to 0.5 is "acceptable", and an NSE ≤ 0.40 is "unsatisfactory". The closer R^2 is to 1, the stronger the positive correlation. Specifically, the value of R^2 can be interpreted as: $R^2 = 1$ is "very good", $0.8 \leq R^2 \leq 1$ is "good", $0.6 \leq R^2 \leq 0.8$ is "satisfactory", $R^2 < 0.6$ is "weak", $R^2 = 0$ is "inefficient", and $R^2 < 0$ is "Invalid" (Vishwakarma et al., 2023; Mirzania et al., 2023). WIA ranges from 0 to 1. Large WIA indicates high degree of agreement between the predicted and measured data. LM is a more advanced and powerful metric than both WIA and NSE, which utilizes the adjustment of comparison in WIA and NSE evaluation. The LM is ranging from $-\infty$ to 1. The closer the LM value is to 1, the better the model. The smaller the LM value, the greater the difference between the observed and predicted values. Negative values indicate the inefficiency of the model in prediction of the variation in the observation.

4. Results and discussion

4.1. The PSO-RF results

In this study, the PSO algorithm was used to optimize the hyperparameters of the RF model. The optimal hyperparameters n_{tree} and p_{try} of the RF model are determined to be 71 and 2, respectively. Figure 8 plots the fitting relationship between experimental results and predicted results for training and test data samples using the proposed PSO-RF model.

As can be seen from Figure 8, the predicted results of PSO-RF model agreement well with the measured results, and the RMSE, MAE, R^2, NSE, WIA and LM values of the PSO-RF model are 1.529 kN, 0.942 kN, 0.986, 0.984, 0.996 and 0.892, respectively, for the training datasets and 2.672 kN, 1.967 kN, 0.963, 0.961, 0.989 and 0.761, respectively, for the test datasets.

4.2. The GEP results

The bond strength calculation formula obtained by GEP is shown in Eqn (26). The optimal parameters used in this study were listed in Table 4. The six statistical indices of the GEP model are shown in Table 5. Figure 9 plots the fitting relationship between experimental results and predicted results for training and test data samples using the GEP model.

$$P_u = \sqrt[3]{t_f}\cdot G_1 G_2 G_3^{-1},$$
$$\begin{cases} G_1 = 1.614\sqrt{k_\alpha} + k_L - \left(1/k_\alpha + 17.059\right)\cdot\left(1/k_\alpha + D_{\max}\right)/b_f \\ G_2 = k_L + \sqrt[3]{k_L + f_c^{0.791} - 49.034} \\ G_3 = k_L - \exp\left(\sqrt[3]{b_f} - \sqrt[3]{e^{t_0} + 17.372}\right) \end{cases}, \quad (26)$$

where
$t_0 = -18.1t_f^2 + 158.2t_f - 45.2$; $k_L = 3.192\ln L + 0.772b_f^{2/3}$;
$k_\alpha = 10^{-3}E_f t_f / D_{max}$.

Table 4. Optimal parameters of the GEP model

Parameter	Setting	Parameter	Setting
Linking function	multiplication (×)	IS transposition rate	0.3
Gene transposition rate	0.3	RIS transposition rate	0.3
Gene recombination rate	0.3	Mutation rate	0.044
Two-point recombination rate	0.4	One-point recombination rate	0.4

4.3. The MARS results

In this study, an analysis model was established based on the MARS open source code of Jekabsons (2011). The MARS model used parameters t_f, b_f, L, f_t and D_{max}. There are 15 BFs, including six univariate BFs (i.e., C_1, C_2, C_3, C_4, C_5 and C_{12}), seven bivariate BFs (i.e., C_6, C_7, C_8, C_9, C_{10}, C_{11} and C_{13}) and two trivariate BFs (i.e., C_{14} and C_{15}). Thus, the MARS model consists of a linear combination of 15 BFs and one constant term, which can be written as Eqns (27) and (28). The six statistical indices of the MARS model are shown in Table 5. Figure 10 plots the fitting relationship between experimental results and predicted results for training and test data samples using the MARS model.

$$
\begin{aligned}
C_1 &= BF\left(t_f \mid s=-1,0.7835,1.4,4.7\right),\\
C_2 &= BF\left(b_f \mid s=+1,14.5,19,34.5\right),\\
C_3 &= BF\left(b_f \mid s=-1,14.5,19,34.5\right),\\
C_4 &= BF\left(L \mid s=+1,67.5,115,657.5\right),\\
C_5 &= BF\left(L \mid s=-1,67.5,115,657.5\right),\\
C_6 &= C_4 \cdot BF\left(t_f \mid s=+1,0.125,0.167,0.7835\right),\\
C_7 &= C_4 \cdot BF\left(t_f \mid s=-1,0.125,0.167,0.7835\right),\\
C_8 &= C_1 \cdot BF\left(f_t \mid s=+1,1.66,2.3,4.3\right),\\
C_9 &= C_1 \cdot BF\left(f_t \mid s=-1,1.66,2.3,4.3\right),\\
C_{10} &= C_4 \cdot BF\left(D_{max} \mid s=+1,8.625,12.5,13.75\right),\\
C_{11} &= C_4 \cdot BF\left(D_{max} \mid s=-1,8.625,12.5,13.75\right),\\
C_{12} &= BF\left(b_f \mid s=+1,34.5,50,62.5\right),\\
C_{13} &= C_1 \cdot BF\left(b_f \mid s=-1,62.5,75,137.5\right),\\
C_{14} &= C_6 \cdot BF\left(D_{max} \mid s=+1,13.75,15,23.5\right),\\
C_{15} &= C_6 \cdot BF\left(D_{max} \mid s=-1,13.75,15,23.5\right).
\end{aligned}
\tag{27}
$$

$$
\begin{aligned}
y = {} & 12.598 - 14.911C_1 + 0.46865C_2 - 1.1657C_3 + \\
& 0.0022771C_4 - 0.043494C_5 + 0.024965C_6 - \\
& 0.27699C_7 + 1.5883C_8 + 4.5804C_9 - 0.00099018C_{10} + \\
& 0.02103C_{11} - 0.24217C_{12} + 0.1186C_{13} - 0.0018196C_{14} - \\
& 0.0023322C_{15}.
\end{aligned}
\tag{28}
$$

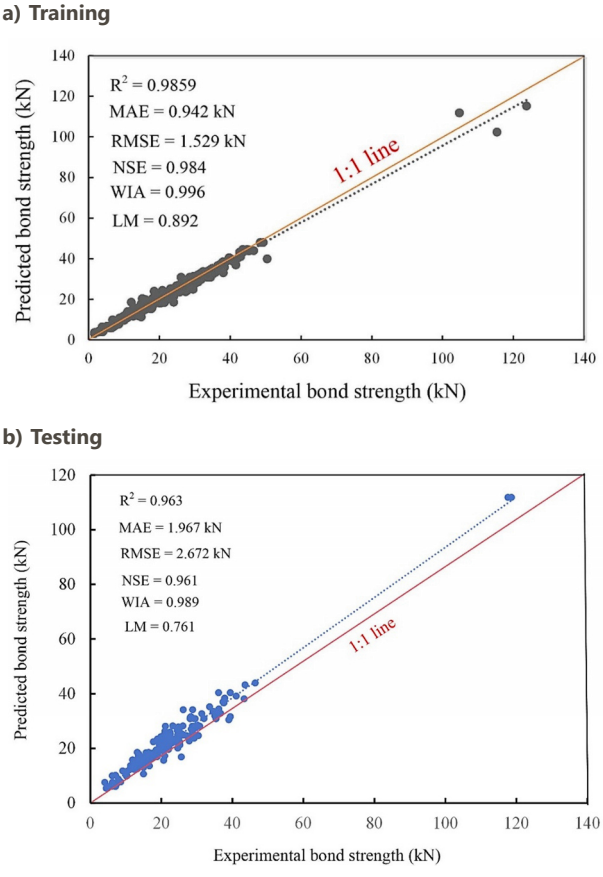

Figure 8. Relationship between the experimental and predicted bond strength of the PSO-RF model

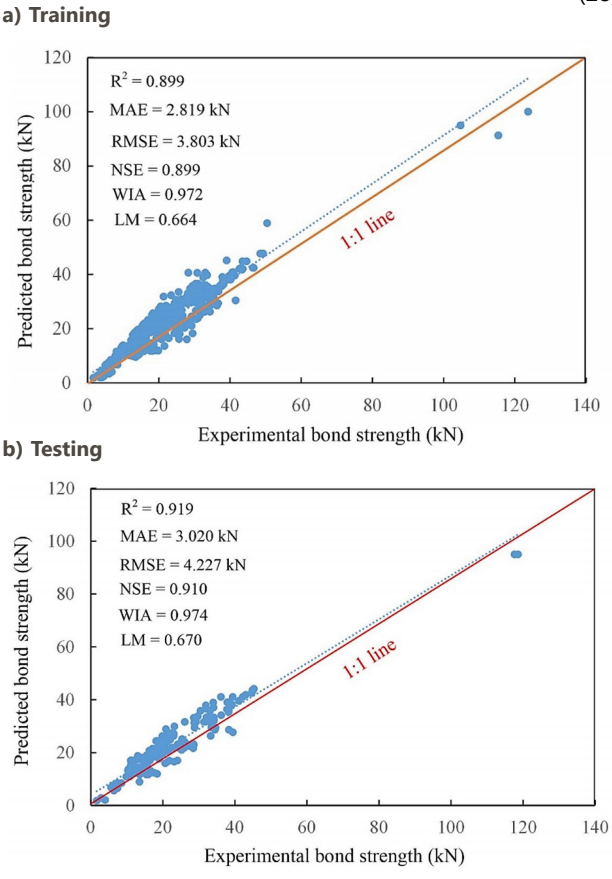

Figure 9. Relationship between the experimental and predicted bond strength of the GEP model

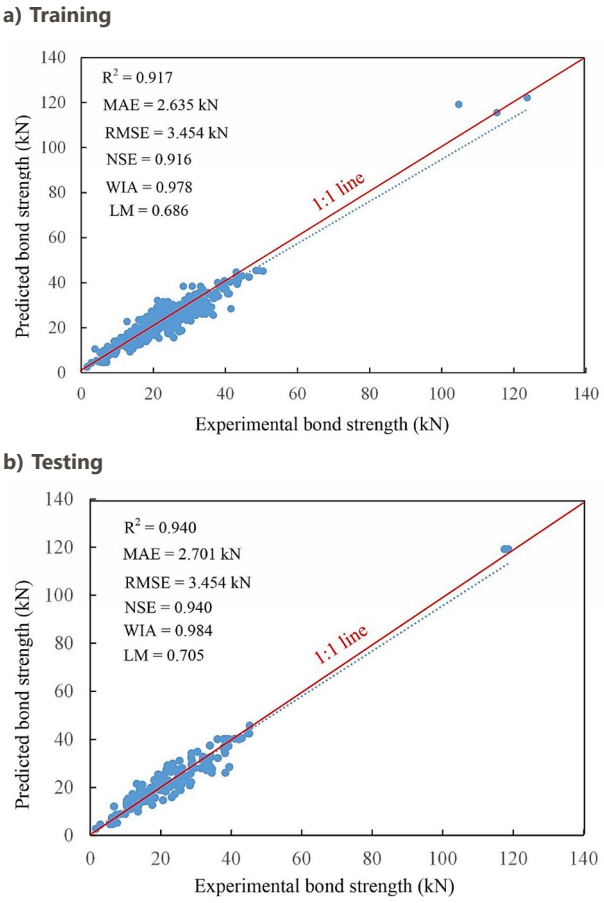

Figure 10. Relationship between the experimental and predicted bond strength of the MARS model

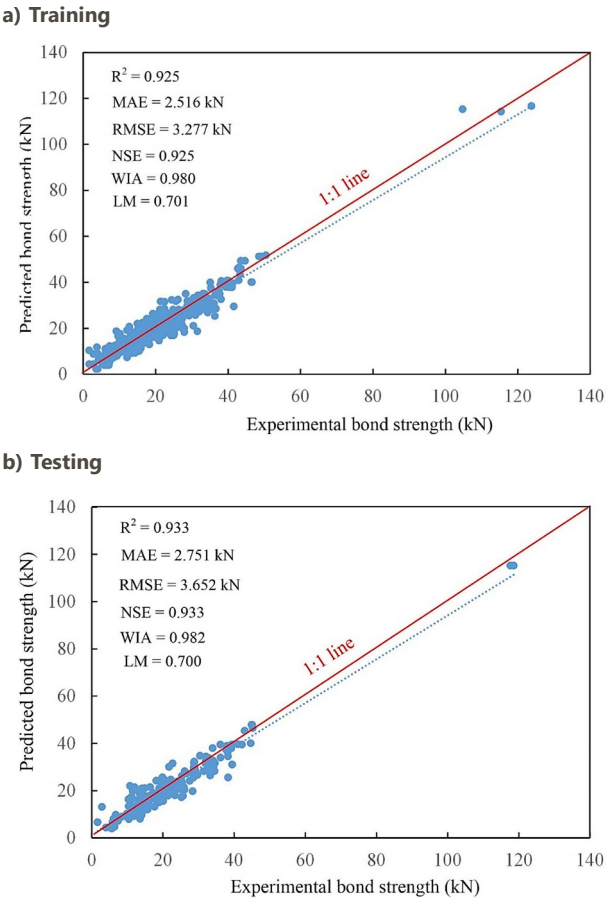

Figure 11. Relationship between the experimental and predicted bond strength of the WNN model

4.4. The WNN results

In this study, there are 10 parameters (i.e., f_c, f_t, b_c, D_{max}, f_{Ft}, t_f, E_f, f_{At}, L and b_f) were used as the input variables, therefore, the number of neurons in the input layer is 10. The optimal number of hidden neurons was determined to be 15 by trial and error. The six statistical indices of the WNN model are shown in Table 5. Figure 11 plots the fitting relationship between experimental results and predicted results for training and test data samples using the WNN model.

4.5. Performance comparison among different models

The prediction performance comparison of these 16 models is shown in Table 5. As can be seen from Table 5, the accuracy of PSO-RF model is the best among the 16 models. For example, the RMSE, MAE, R^2, NSE, WIA and LM values of the PSO-RF model are 1.529 kN, 0.942 kN, 0.986, 0.984, 0.996 and 0.892, respectively, for the training datasets and 2.672 kN, 1.967 kN, 0.963, 0.961, 0.989 and 0.761, respectively, for the test datasets. It can be seen that regardless of the training or testing datasets, the PSO-RF model has the highest R^2, NSE, WIA, LM and the lowest MAE and RMSE, indicating that the PSO-RF model has the best performance.

In addition, it can be seen that the second-best performing model is RF. For example, the RMSE, MAE, R^2, NSE, WIA and LM values of the RF model are 2.386 kN, 1.421 kN, 0.971, 0.961, 0.989 and 0.832, respectively, for the training datasets and 3.606 kN, 2.194 kN, 0.941, 0.932, 0.980 and 0.756, respectively, for the test datasets. Compared with the RF model, the MAE and RMSE values of training and test sets of the PSO-RF were decreased by 33.71% and 35.92%; 10.35% and 25.9%, respectively; while the R^2, NSE, WIA and LM values of the PSO-RF were increased by 1.54%, 2.39%, 0.71% and 7.21%, respectively, for the training datasets and 2.34%, 3.11%, 0.92% and 0.66%, respectively, for the test datasets. The results show that the PSO algorithm has a good effect on the hyperparameter optimization of the RF model.

Among GMDH, GEP, MARS and WNN models, the WNN model has the best performance on the training data set. However, for the test datasets, the best-performing model is the MARS model. For example, the RMSE, MAE, R^2, NSE, WIA and LM values of the WNN model for the training datasets are 3.277 kN, 2.516 kN, 0.925, 0.925, 0.98 and 0.701, respectively. The RMSE, MAE, R^2, NSE, WIA and LM values of the MARS model for the test datasets are 3.454 kN, 2.701 kN, 0.94, 0.94, 0.984 and 0.705, respectively. The training effect difference between GMDH and GEP models is very small and can be considered to be almost the same.

In addition, it can be seen that the accuracy of these ten existing empirical models is generally low. For example, the RMSE, MAE, R^2, NSE, WIA and LM values of the Maeda et al. (1999) model are 257.4 kN, 134.5 kN, 0.587, –396.803, 0.125 and –15.404, respectively, for the training datasets and 170.1 kN, 70.35 kN, 0.265, –243.403, 0.113 and –6.339, respectively, for the test datasets. The main reasons for the low prediction accuracy of these ten empirical models are (1) the coefficients in the formulas are determined by the linear regression analysis of experimental data, and (2) the scope of application is not large enough.

If only in terms of the R^2 values, for the training datasets, the performance rank could be listed as follows: PSO-RF > RF > WNN > MARS > GDMH > GEP > JCI (2003) > Accardi et al. (2007) > Khalifa et al. (1998) > Neubauer and Rostásy (1997) > Niedermeier (1996) > Maeda et al. (1999) > Chen and Teng (2001) > Dai et al. (2005) > Hiroyuki and Wu (1997) > Yang et al. (2001). However, for the test datasets, the performance rank could be listed as follows: PSO-RF > RF > MARS > WNN > GEP > GMDH > Accardi et al. (2007) > Niedermeier (1996) > Dai et al. (2005) > JCI (2003) > Neubauer and Rostásy (1997) > Chen and Teng (2001) > Hiroyuki and Wu (1997) > Yang et al. (2001) > Khalifa et al. (1998) > Maeda et al. (1999). It can be seen that the R^2, NSE, WIA and LM values of the PSO-RF model are the highest and the MAE and RMSE values are the lowest in both the training datasets and the test datasets, and the PSO-RF model performs the best. Therefore, it can be concluded that the proposed PSO-RF model has the best comprehensive performance in predicting the bond strength of FRP-to-concrete.

In order to more intuitively compare the performance of various models, the results in Table 5 are also presented graphically. Since the statistical index values calculated by these six AI models differ by many orders of magnitude from those calculated by the existing ten empirical models, and the results predicted by these empirical models have large errors, this study only presents the comparison results of these six AI models in the form of graphs, as shown in Figures 12 and 13. As can be seen from Figure 12, the closer the Taylor chart model is to the observed value, the better the model effect is. It is found that in the training stage and the test stage, the PSO-RF model has the closest distance from the observed value and the best effect. In addition, it can be seen from Figure 13 that regardless of the training or testing datasets, the PSO-RF model has the highest R^2, NSE, WIA, LM and the lowest MAE and RMSE, indicating that the PSO-RF model has the best performance.

4.6. Sensitivity analysis

To investigate the influence of the input parameters (i.e., f_c, f_t, b_c, D_{max}, f_{Ft} , t_f , E_f , f_{At}, L, b_f) on the prediction performance, ten hybrid PSO-RF models were developed with different kinds of inputs. The statistical indices of these PSO-RF models on the training and test data sets are shown in Table 6.

Table 5. Performance comparison among different models

Model	Training datasets						Testing datasets					
	RMSE/kN	MAE/kN	R^2	NSE	WIA	LM	RMSE/kN	MAE/kN	R^2	NSE	WIA	LM
PSO-RF	1.529	0.942	0.986	0.984	0.996	0.892	2.672	1.967	0.963	0.961	0.989	0.761
RF	2.386	1.421	0.971	0.961	0.989	0.832	3.606	2.194	0.941	0.932	0.980	0.756
GMDH	3.934	2.953	0.907	0.907	0.975	0.640	4.803	3.647	0.855	0.805	0.938	0.620
GEP	3.803	2.819	0.899	0.899	0.972	0.664	4.227	3.020	0.919	0.910	0.974	0.670
MARS	3.454	2.635	0.917	0.916	0.978	0.686	3.454	2.701	0.940	0.940	0.984	0.705
WNN	3.277	2.516	0.925	0.925	0.980	0.701	3.652	2.751	0.933	0.933	0.982	0.700
JCI (2003)	519	442.2	0.618	–1622	0.052	–52.916	388.6	305.9	0.696	–1274.13	0.069	–30.916
Maeda et al. (1999)	257.4	134.5	0.587	–396.803	0.125	–15.404	170.1	70.35	0.265	–243.403	0.113	–6.339
Dai et al. (2005)	1143	1001	0.554	–7846.636	0.023	–121.168	923.1	767.5	0.707	–7193.89	0.029	–79.066
Accardi et al. (2007)	5746	4982	0.614	–198276.405	0.005	–606.521	4501	3674	0.731	–171082.15	0.006	–382.272
Khalifa et al. (1998)	183.7	94.29	0.613	–107.469	0.165	–3.56	113.3	43.71	0.268	–181.337	0.174	–8.547
Niedermeier (1996)	804.9	694.5	0.587	–3889.407	0.033	–83.684	644.8	525.3	0.718	–3509.594	0.042	–53.798
Yang et al. (2001)	6573	5864	0.246	–259464.486	0.003	–714.103	6301	4832	0.405	–335268.359	0.004	–503.129
Neubauer and Rostásy (1997)	899.9	797.7	0.596	–4862.496	0.029	–96.261	697.8	568.6	0.658	–4109.934	0.037	–60.191
Chen and Teng (2001)	675.3	597.6	0.585	–2737.661	0.038	–71.86	500.4	424.8	0.643	–2113.304	0.051	–43.314
Hiroyuki and Wu (1997)	2475	2200	0.377	–36800.365	0.009	–267.299	2172	1776	0.562	–39834.824	0.012	–184.328

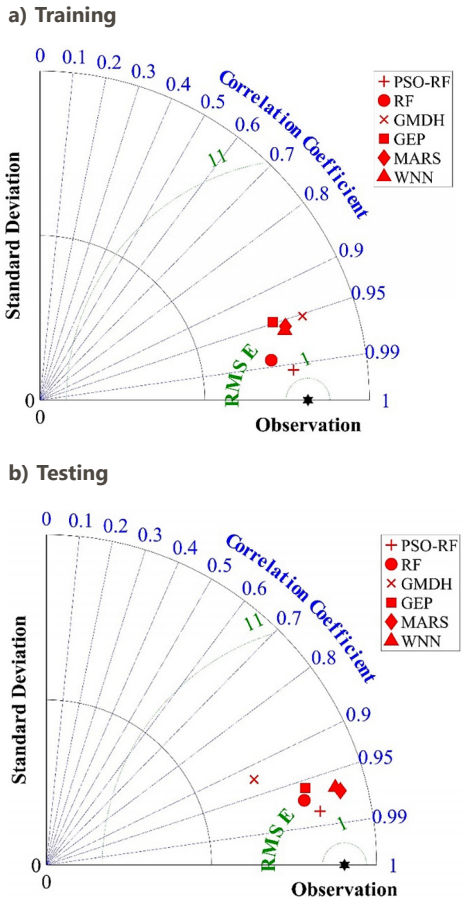

Figure 12. Taylor diagram of six AI models

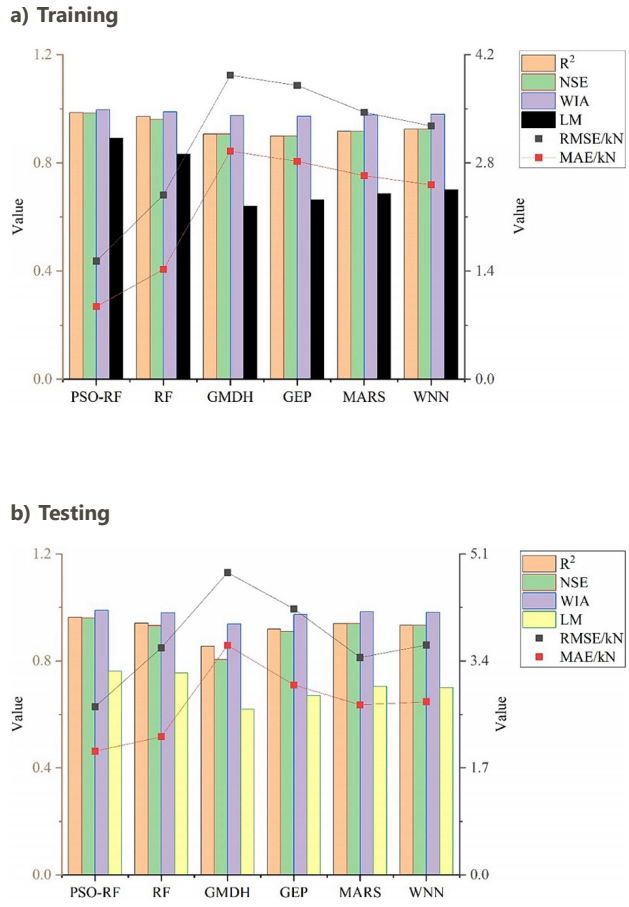

Figure 13. Performance comparison among six AI models

Table 6. Single parameter sensitivity analysis of the PSO-RF model

Model	Training datasets						Testing datasets					
	RMSE/kN	MAE/kN	R^2	NSE	WIA	LM	RMSE/kN	MAE/kN	R^2	NSE	WIA	LM
With all parameters	1.529	0.942	0.986	0.984	0.996	0.892	2.672	1.967	0.963	0.961	0.989	0.761
Without f_c	1.537	0.965	0.979	0.981	0.994	0.885	2.702	1.974	0.958	0.958	0.981	0.753
Without f_t	1.531	0.955	0.981	0.983	0.995	0.890	2.681	1.971	0.961	0.959	0.984	0.759
Without b_c	1.584	0.972	0.974	0.978	0.991	0.878	2.783	1.984	0.949	0.948	0.976	0.743
Without D_{max}	1.574	0.971	0.977	0.979	0.993	0.881	2.727	1.982	0.951	0.952	0.979	0.749
Without f_{Ft}	1.617	1.108	0.970	0.971	0.987	0.869	2.943	1.991	0.927	0.922	0.963	0.704
Without t_f	2.335	1.363	0.967	0.966	0.973	0.841	4.318	2.278	0.914	0.907	0.948	0.694
Without E_f	1.610	1.091	0.971	0.973	0.988	0.873	2.905	1.989	0.936	0.932	0.971	0.716
Without f_{At}	1.587	0.985	0.972	0.974	0.990	0.876	2.813	1.987	0.940	0.942	0.974	0.735
Without L	2.069	1.361	0.968	0.968	0.977	0.846	3.584	2.256	0.916	0.918	0.950	0.699
Without b_f	4.378	2.723	0.883	0.881	0.955	0.687	5.399	3.715	0.807	0.803	0.933	0.569

As observed from Table 6, regardless of the training or testing datasets, the PSO-RF model with all the parameters has the highest R^2, NSE, WIA, LM and the lowest MAE and RMSE, indicating that the PSO-RF model with all the parameters has the best performance.

In addition, it can also be seen from Table 6 that the thickness t_f, bond width b_f, length L, tensile strength f_{Ft} and elastic modulus E_f of FRP have great influence on the bond strength of FRP and concrete. Among them, the bond width of FRP b_f has the most significant influence on the bond strength. For example, the RMSE, MAE, R^2, NSE, WIA and LM values of the PSO-RF model without b_f are 4.378 kN, 2.723 kN, 0.883, 0.881, 0.955 and 0.687, respectively, for the training datasets and 5.399 kN, 3.715 kN, 0.807, 0.803, 0.933 and 0.569, respectively, for the test datasets. Regardless of the training or testing datasets, the PSO-RF model without b_f has the lowest R^2, NSE, WIA, LM and the highest MAE and RMSE, indicating that the bond

width of FRP b_f has the most significant influence on the bond strength. The effect rank of these ten input parameters on the bond strength of FRP-to-concrete is: bond width of FRP b_f > thickness of FRP t_f > bond length of FRP L > tensile strength of FRP f_{Ft} > elastic modulus of FRP E_f > tensile strength of adhesive f_{At} > width of concrete specimen b_c > maximum aggregate size of concrete D_{max} > compressive strength of concrete f_c > tensile strength of concrete f_t , which is consistent with the Pearson analysis results (as shown in Table 2).

4.7. Limitations of the study and future research

Although the proposed PSO-RF model has high accuracy, it also has some limitations. For example, the proposed model is suitable for the current range of data and parameters, and cannot guarantee to provide high prediction accuracy when the data is outside the predetermined range. The accuracy of the proposed PSO-RF model can still be improved and more data samples are needed for calibration. In addition, the RF model in this study was optimized using only PSO and can be optimized in the future using other evolutionary algorithms such as GAs, evolution strategies, ant colony optimization, simulated annealing, and biogeography-based optimization.

For the MARS, GEP, GMDH and WNN models, although the prediction accuracy of these models is also relatively high, the above evolutionary algorithms can also be used to optimize these models in future work.

The prediction accuracy of these empirical models is relatively low. In future work, more data are needed to validate these empirical formulas or to optimize them using evolutionary algorithms to determine their reasonable range of applications.

5. Conclusions

In this study, a novel hybrid PSO-RF model was proposed to predict the bond strength of FRP-to-concrete. The PSO algorithm was used to optimize the hyperparameters of the RF model. The proposed model was compared with other machine learning models as well as ten empirical equations. The results show that the predicted results of PSO-RF model are in good agreement with the measured results, and the RMSE, MAE, R^2, NSE, WIA and LM values of the PSO-RF model are 1.529 kN, 0.942 kN, 0.986, 0.984, 0.996 and 0.892, respectively, for the training datasets and 2.672 kN, 1.967 kN, 0.963, 0.961, 0.989 and 0.761, respectively, for the test datasets. Regardless of the training or testing datasets, the PSO-RF model has the highest R^2, NSE, WIA, LM and the lowest MAE and RMSE. According to the value range of these statistical indices, it can be concluded that the proposed PSO-RF model has the best comprehensive performance in predicting the bond strength of FRP-to-concrete.

If only in terms of the R^2 values, for the training datasets, the performance rank could be listed as follows: PSO-RF > RF > WNN > MARS > GDMH > GEP > JCI (2003) > Accardi et al. (2007) > Khalifa et al. (1998) > Neubauer and Rostásy (1997) > Niedermeier (1996) > Maeda et al. (1999) > Chen and Teng (2001) > Dai et al. (2005) > Hiroyuki and Wu (1997) > Yang et al. (2001). However, for the test datasets, the performance rank could be listed as follows: PSO-RF > RF > MARS > WNN > GEP > GMDH > Accardi et al. (2007) > Niedermeier (1996) > Dai et al. (2005) > JCI (2003) > Neubauer and Rostásy (1997) > Chen and Teng (2001) > Hiroyuki & Wu (1997) > Yang et al. (2001) > Khalifa et al. (1998) > Maeda et al. (1999).

The sensitivity analysis results show that the PSO-RF model without b_f has the lowest R^2, NSE, WIA, LM and the highest MAE and RMSE, indicating that the bond width of FRP b_f has the most significant influence on the bond strength. The effect rank of these ten input parameters on the bond strength of FRP-to-concrete is: bond width of FRP b_f > thickness of FRP t_f > bond length of FRP L > tensile strength of FRP f_{Ft} > elastic modulus of FRP E_f > tensile strength of adhesive f_{At} > width of concrete specimen b_c > maximum aggregate size of concrete D_{max} > compressive strength of concrete f_c > tensile strength of concrete f_t, which is consistent with the Pearson analysis results.

One limitation of this study is that the proposed model is only applicable to the current range of data and parameters, and cannot guarantee high prediction accuracy when the data exceeds the predetermined range. Therefore, the accuracy of the proposed PSO-RF model still needs to be improved, and more data samples are needed for calibration.

Authorship contribution statement

Li Tao: Conceptualization, Methodology, Writing-original draft. Xinhua Xue: Conceptualization, Methodology, Writing-reviewing, Editing, Supervision.

Funding

No funding is associated with this article.

Data availability statement

Data will be made available on reasonable request.

Conflict of interest

The authors declare that they have no conflict of interest.

Ethical approval

This article does not contain any studies with human participants or animals performed by any of the authors.

References

Accardi, M., Cucchiara, C., & La Mendola, L. (2007). Bond behavior between CFRP strips and calcarenite stone. In *Proceedings of the 6th International Conference on Fracture Mechanics of Concrete and Concrete Structures*, Catania, Italy.

Alam, M. A., Onik, S. A., & Bin Mustapha, K. N. (2020). Crack based bond strength model of externally bonded steel plate and CFRP laminate to predict debonding failure of shear strengthened RC beams. *Journal of Building Engineering*, *27*, Article 100943. https://doi.org/10.1016/j.jobe.2019.100943

Al-Saadi, N. T. K., Mohammed, A, & Al-Mahaidi, R. (2018). Bond performance of NSM CFRP strips embedded in concrete using direct pull-out testing with cementitious adhesive made with graphene oxide. *Construction and Building Materials*, *162*, 523–533. https://doi.org/10.1016/j.conbuildmat.2017.12.050

Ascione, F., Lamberti, M., Napoli, A., Razaqpur, A. G., & Realfonzo, R. (2019). Modeling SRP-concrete interfacial bond behavior and strength. *Engineering Structures*, *187*, 220–230. https://doi.org/10.1016/j.engstruct.2019.02.050

Barham, W. S., Obaidat, Y. T., & Al-Maabreh, A. I. (2019). Effect of aggregate size on the bond behavior between carbon fiber-reinforced polymer sheets and concrete. *Journal of Materias in Civil Engineering*, *31*(12), Article 04019295. https://doi.org/10.1061/(ASCE)MT.1943-5533.0002950

Barris, C., Correia, L., & Sena-Cruz, J. (2018). Experimental study on the bond behaviour of a transversely compressed mechanical anchorage system for externally bonded reinforcement. *Composite Structures*, *200*, 217–228. https://doi.org/10.1016/j.compstruct.2018.05.084

Bakis, C. E., Uppuluri, V. S., Nanni, A., & Boothby, T. E. (1998). Analysis of bonding mechanisms of smooth and lugged FRP rods embedded in concrete. *Composites Science and Technology*, *58*(8), 1307–1319. https://doi.org/10.1016/S0266-3538(98)00016-5

Breiman, L. (2001). Random forests. *Machine Learning*, *45*, 5–32. https://doi.org/10.1023/A:1010933404324

Cascardi, A., Micelli, F., & Aiello, M. A. (2017). An artificial neural networks model for the prediction of the compressive strength of FRP-confined concrete circular columns. *Engineering Structures*, *140*, 199–208. https://doi.org/10.1016/j.engstruct.2017.02.047

Chróścielewski, J., Ferenc, T., Mikulski, T., Miśkiewicz, M., & Pyrzowski, Ł. (2019). Numerical modelling and experimental validation of full-scale segment to support design of novel GFRP footbridge. *Composite Structures*, *213*, 299–307. https://doi.org/10.1016/j.compstruct.2019.01.089

Chen, J. F., & Teng, J. (2001). Anchorage strength models for FRP and steel plates bonded to concrete. *Journal of Structural Engineering*, *127*(7), 784–791. https://doi.org/10.1061/(ASCE)0733-9445(2001)127:7(784)

Chen, S. Z., Zhang, S. Y., Han, W. S., & Wu, G. (2021). Ensemble learning based approach for FRP-concrete bond strength prediction. *Construction and Building Materials*, *302*, Article 124230. https://doi.org/10.1016/j.conbuildmat.2021.124230

Correial, L., Barris, C., Franca, P., & Sena-Curz, J. (2019). Effect of temperature on bond behavior of externally bonded FRP laminates with mechanical end anchorage. *Journal of Composites for Construction*, *23*(5), Article 04019036. https://doi.org/10.1061/(ASCE)CC.1943-5614.0000961

Czaderski, C., Soudki, K., & Motavalli, M. (2010). Front and side view image correlation measurements on FRP to concrete pull-off bond tests. *Journal of Composites for Construction*, *14*(4), 451–463. https://doi.org/10.1061/(ASCE)CC.1943-5614.0000106

Dai, J., Ueda, T., & Sato, Y. (2005). Development of the nonlinear bond stress–slip model of fiber reinforced plastics sheet–concrete interfaces with a simple method. *Journal of Composites for Construction*, *9*(1), 52–62. https://doi.org/10.1061/(ASCE)1090-0268(2005)9:1(52)

Dai, Y., Khandelwal, M., Qiu, Y., Zhou, J., Monjezi, M., & Yang, P. X. (2022). A hybrid metaheuristic approach using random forest and particle swarm optimization to study and evaluate backbreak in open-pit blasting. *Neural Computing and Applications*, *34*, 6273–6288. https://doi.org/10.1007/s00521-021-06776-z

Daneshvar, D., & Behnood, A. (2020). Estimation of the dynamic modulus of asphalt concretes using random forests algorithm. *International Journal of Pavement Engineering*, *23*(2), 250–260. https://doi.org/10.1080/10298436.2020.1741587

Daud, R. A., Cunningham, L. S., & Wang, Y. C. (2015). Static and fatigue behaviour of the bond interface between concrete and externally bonded CFRP in single shear. *Engineering Structures*, *97*, 54–67. https://doi.org/10.1016/j.engstruct.2015.03.068

Daud, R. A., Cunningham, L. S., Wang, & Y. C. (2017). New model for post-fatigue behaviour of CFRP to concrete bond interface in single shear. *Composite Structures*, *163*, 63–76. https://doi.org/10.1016/j.compstruct.2016.12.029

Friedman, J. H. (1991). Multivariate adaptive regression splines. *Annals of Statistics*, *19*(1), 1–67. https://doi.org/10.1214/aos/1176347963

Ferreira, C. (2001). Gene expression programming: a new adaptive algorithm for solving problems. *Complex and Intelligent Systems*, *13*, 87–129. https://doi.org/10.48550/arXiv.cs/0102027

Garzon-Roca, J., Sena-Cruz, J. M., Fernandes, P., & Xavier, J. (2015). Effect of wet-dry cycles on the bond behaviour of concrete elements strengthened with NSM CFRP laminate strips. *Composite Structures*, *132*, 331–340. https://doi.org/10.1016/j.compstruct.2015.05.053

Ghorbani, M., Mostofinejad, D., & Hosseini, A. (2017). Experimental investigation into bond behavior of FRP-to-concrete under mixed-mode I/II loading. *Construction and Building Materials*, *132*, 303–312. https://doi.org/10.1016/j.conbuildmat.2016.11.057

Haddad, R. H., Al-Rousan, R., Ghanma, L., & Nimri, Z. (2015). Modifying CFRP-concrete bond characteristics from pull-out testing. *Magazine of Concrete Ressearch*, *67*(13), 707–717. https://doi.org/10.1680/macr.14.00271

Hadigheh, S., Gravina, R., & Setunge, S. (2015). Identification of the interfacial fracture mechanism in the FRP laminated substrates using a modified single lap shear test set-up. *Engineering Fracture Mechanics*, *134*, 317–329. https://doi.org/10.1016/j.engfracmech.2014.12.001

Hiroyuki, Y., & Wu, Z. S. (1997). Analysis of debonding fracture properties of CFS strengthened RC member subject to tension. In *Proceedings of 3rd International Symposium on the Non-Metallic (FRP) Reinforcement for Concrete Structures*, The Japan Concrete Institute, Japan.

Irshidat, M. R., & Al-Saleh, M. H. (2016). Effect of using carbon nanotube modified epoxy on bond-slip behavior between concrete and FRP sheets. *Construction and Building Materials*, *105*, 511–518. https://doi.org/10.1016/j.conbuildmat.2015.12.183

Ivakhnenko, A. G. (1971). Polynomial theory of complex systems. *IEEE Transactions on Systems, Man, and Cybernetics*, *4*, 364–378. https://doi.org/10.1109/TSMC.1971.4308320

Jahangir, H., & Eidgahee, D. R. (2021). A new and robust hybrid artificial bee colony algorithm – ANN model for FRP-concrete bond strength evaluation. *Composite Structures*, 257, Article 113160. https://doi.org/10.1016/j.compstruct.2020.113160

Japan Concrete Institute. (2003). *Technical report of Technical Committee on retrofit technology*.

Jekabsons, G. (2011). *ARESLab: Adaptive regression splines toolbox for Matlab/Octave*. http://www.cs.rtu.lv/jekabsons/

Khalifa, A., Gold, W. J., Nanni, A., & Abdel Aziz, M. I. (1998). Contribution of externally bonded FRP to shear capacity of RC flexural members. *Journal of Composites for Construction*, *2*(4), 195–202. https://doi.org/10.1061/(ASCE)1090-0268(1998)2:4(195)

Legates, D. R., & McCabe, G. J. (1999). Evaluating the use of "goodness-of-fit" measures in hydrologic and hydroclimatic model validation. *Water Resources Research*, *35*(1), 233–241. https://doi.org/10.1029/1998WR900018

Luat, N. V., Shin, J., & Lee, K. (2021). Ultimate axial capacity prediction of CCFST columns using hybrid intelligence models-a new approach. *Steel and Composite Structures*, *40*(3), 461–479. https://doi.org/10.12989/scs.2021.40.3.461

Maeda, T., Asano, Y., Sato, Y., Ueda, T., & Kakuta, Y. (1999). A study on bond mechanism of carbon fiber sheet. In *Proceedings of the 3rd International Symposium on Non-Metallic* (*FRP*) *Reinforcement for Concrete Structures* (pp. 279–286), Sapporo, Japan.

Mirzania, E., Vishwakarma, D. K., Bui, Q. A. T., Band, S. S., & Dehghani, R. (2023). A novel hybrid AIG-SVR model for estimating daily reference evapotranspiration. *Arabian Journal of Geosciences*, *16*, Article 301. https://doi.org/10.1007/s12517-023-11387-0

Murad, Y., Ashteyat, A., & Hunaifat, R. (2019). Predictive model to the bond strength of FRP-to-concrete under direct pullout using gene expression programming. *Journal of Civil Engineering and Management*, *25*(8), 773–784. https://doi.org/10.3846/jcem.2019.10798

Nash, J. E., & Sutcliffe, J. V. (1970). River flow forecasting through conceptual models part I_A discussion of principles. *Journal of Hydrology*, *10*, 282–290. https://doi.org/10.1016/0022-1694(70)90255-6

Naser, M. Z., Kodur, V., Thai, H. T., Hawileh, R., Abdalla, J., & Degtyarev, V. V. (2021). *StructuresNet* and *FireNet*: Benchmarking datasets and machine learning algorithms in structural and fire engineering domains. *Journal of Building Engineering*, *44*, Article 102977. https://doi.org/10.1016/j.jobe.2021.102977

Nerilli, F., & Vairo, G. (2018). Experimental investigation on the debonding failure mode of basalt-based FRP sheets from concrete. *Composites Part B: Engineering*, *153*, 205–216. https://doi.org/10.1016/j.compositesb.2018.07.002

Neubauer, U., & Rostásy, F. S. (1997). Design aspects of concrete structures strengthened with externally bonded CFRP plates. In *Proceedings of the 7th International Conference on Structural Faults and Repairs* (Vol. 2, pp. 109–118). ECS Publications.

Niedermeier, R. (1996). *Stellungnahme zur richtlinie für das verkleben von betonbauteilen durch ankleben von stahllaschen-entwurf*. Technische University, Munich, Germany.

Nilsen, V., Le Pham, T., Hibbard, M., Klager, A., Cramer, S. M., & Morgan, D. (2019). Prediction of concrete coefficient of thermal expansion and other properties using machine learning. *Construction and Building Materials*, *220*, 587–595. https://doi.org/10.1016/j.conbuildmat.2019.05.006

Ozakkaloglu, T., Fang, C., & Gholampour, A. (2017). Influence of FRP anchor configuration on the behavior of FRP plates externally bonded on concrete members. *Engineering Structures*, *13*, 133–150. https://doi.org/10.1016/j.engstruct.2016.12.005

Pan, J., & Leung, C. K. (2007). Effect of concrete composition on FRP/concrete bond capacity. *Journal of Composites for Construction*, *11*(6), 611–618. https://doi.org/10.1061/(ASCE)1090-0268(2007)11:6(611)

Pei, Z., & Wei, Y. F. (2022). Prediction of the bond strength of FRP-to-concrete under direct tension by ACO-based ANFIS approach. *Composite Structures*, *282*, Article 115070. https://doi.org/10.1016/j.compstruct.2021.115070

Peng, H., Hao, H., Zhang, J., Liu, Y., & Cai, C. S. (2015). Experimental investigation of the bond behavior of the interface between near-surface-mounted CFRP strips and concrete. *Construction and Building Materials*, *96*, 11–19. https://doi.org/10.1016/j.conbuildmat.2015.07.156

Siwowski, T., Rajchel, M., & Kulpa, M. (2019). Design and field evaluation of a hybrid FRP composite – Lightweight concrete road bridge. *Composite Structures*, *230*, Article 111504. https://doi.org/10.1016/j.compstruct.2019.111504

Vishwakarma, D. K., Kuriqi, A., Abed, S. A., Kishore, G., Al-Ansari, N., Pandey, K., Kumar, P., Kushwaha, N. L., & Jewel, A. (2023). Forecasting of stage-discharge in a non-perennial river using machine learning with gamma test. *Heliyon*, *9*, Article e16290. https://doi.org/10.1016/j.heliyon.2023.e16290

Wan, B., Jiang, C., & Wu, Y. F. (2018). Effect of defects in externally bonded FRP reinforced concrete. *Construction and Building Materials*, *172*, 63–76. https://doi.org/10.1016/j.conbuildmat.2018.03.217

Willmott, C. J. (1981). On the validation of models. *Physical Geography*, *2*(2), 184–194. https://doi.org/10.1080/02723646.1981.10642213

Yang, Y. X.,Yue, Q. R., & Hu, Y. C. (2001). Experimental study on bond performance between carbon fiber sheets and concrete. *Journal of Building Structures*, *22*, 36–42 (in Chinese).

Yuan, C., Chen, W. S., Pham, T. M., Cui, J., Shi, Y. C., & Hao, H. (2019). Effect of aggregate size on the dynamic interfacial bond behaviour between basalt fiber reinforced polymer sheets and concrete. *Construction and Building Materials*, *227*, Article 116584. https://doi.org/10.1016/j.conbuildmat.2019.07.310

Zhang, Q., & Benveniste, A. (1992). Wavelet networks. *IEEE Transactions on Neural Networks and Learning Systems*, *3*(6), 889–898. https://doi.org/10.1109/72.165591

Zhang, J. F., & Wang, Y. H. (2021). Evaluating the bond strength of FRP-to-concrete composite joints using metaheuristic-optimized least-squares support vector regression. *Neural Computing and Applications*, *33*, 3621–3635. https://doi.org/10.1007/s00521-020-05191-0

Zhang, F., Wang, C. X., Liu, J., Zou, X. X., Sneed, L. H., Bao, Y., & Wang, L. B. (2023). Prediction of FRP-concrete interfacial bond strength based on machine learning. *Engineering Structures*, *274*, Article 115156. https://doi.org/10.1016/j.engstruct.2022.115156

APPENDIX

Abbreviations

FRP	Fiber-reinforced polymer;
AI	Artificial intelligence;
ANNs	Artificial neural networks;
ANFIS	Adaptive neuro-fuzzy inference system;
SVM	Support vector machine;
LSSVM	Least squares support vector machine;
M5MT	M5 model tree;
MARS	Multivariate adaptive regression splines;
RMSE	Root mean squared error;
MAE	Mean absolute error;
R^2	Coefficient of determination;
NSE	Nash-Sutcliffe efficiency coefficient;
WIA	Willmott's Index of Agreement;
LM	Legates-McCabe's Index;
P_u	Bond strength of FRP-to-concrete;
RF	Random forest;
RT	Random tree;
GA	Genetic algorithm;
GP	Genetic programming;
PSO	Particle swarm optimization;
f_c	Compressive strength of concrete;
f_t	Tensile strength of concrete;
b_c	Width of concrete specimen;
D_{max}	Maximum aggregate size of concrete;
f_{Ft}	Tensile strength of FRP;
t_f	Thickness of FRP;
E_f	Elastic modulus of FRP;
f_{At}	Tensile strength of adhesive;
L	Bond length of FRP;
b_f	Bond width of FRP.